Rapid Communications

Editors' Suggestion

Anomalous charge noise in superconducting qubits

B. G. Christensen, ¹ C. D. Wilen, ² A. Opremcak, ² J. Nelson, ³ F. Schlenker, ² C. H. Zimonick, ² L. Faoro, ^{2,4} L. B. Ioffe, ^{2,4} Y. J. Rosen, ⁵ J. L. DuBois, ⁵ B. L. T. Plourde, ³ and R. McDermott ²

¹Intelligence Community Postdoctoral Research Fellowship Program, University of Wisconsin-Madison, Madison, Wisconsin 53706, USA

²Department of Physics, University of Wisconsin-Madison, Madison, Wisconsin 53706, USA

³Department of Physics, Syracuse University, Syracuse, New York 13244, USA

⁴Laboratoire de Physique Theorique et Hautes Energies, Sorbonne Universite, UMR 7589 CNRS, Tour 13, 5eme Etage, 4 Place Jussieu, F-75252 Paris 05, France

⁵Condensed Matter and Materials Division, Lawrence Livermore National Laboratory, Livermore, California 94550, USA



(Received 31 May 2019; revised manuscript received 3 October 2019; published 24 October 2019)

We have used Ramsey tomography to characterize charge noise in a weakly charge-sensitive superconducting qubit. We find a charge noise that scales with frequency as $1/f^{\alpha}$ over five decades with $\alpha=1.93$ and a magnitude $S_q(1~{\rm Hz})=2.9\times10^{-4}~e^2/{\rm Hz}$. The noise exponent and magnitude of the low-frequency noise are much larger than those seen in prior work on single electron transistors, yet are consistent with reports of frequency noise in other superconducting qubits. Moreover, we observe frequent large-amplitude jumps in offset charge exceeding 0.1e; these large discrete charge jumps are incompatible with a picture of localized dipolelike two-level fluctuators. The data reveal an unexpected dependence of charge noise on device scale and suggest models involving either charge drift or fluctuating patch potentials.

DOI: 10.1103/PhysRevB.100.140503

Superconducting quantum circuits are a leading physical platform for scalable quantum computing, with small-scale qubit arrays nearing the threshold of quantum supremacy [1,2]. The progress of recent years has been enabled by designs that isolate the qubit mode from sources of noise and dissipation inherent in the materials used to realize the device. However, these approaches entail design compromises that could impede continued scaling. For example, the highly successful transmon design [3] achieves exponential insensitivity against charge noise at the expense of reduced anharmonicity. As a result, leakage out of the computational subspace represents a significant problem for large-scale transmon arrays, as it cannot be mitigated with standard error correction codes [4]. At the same time, there are proposals for new qubit designs that provide protection against noise at the hardware level, including charge-parity qubits [5,6], fluxon pair qubits [7], and $0-\pi$ qubits [8]. However, in many of these implementations one needs accurate control over the offset charge environment. These considerations motivate a detailed study of charge noise in modern superconducting qubit circuits.

Excess low-frequency charge noise (or equivalently electric field noise) impacts a wide range of physical systems, including nitrogen-vacancy centers [9], trapped ions [10], semiconducting quantum dots [11], and single electron transistors (SETs) [12–20], and there has been extensive prior work to understand the origin and scaling of the noise. Previous measurements in SET devices and first-generation charge qubits [21] showed a 1/f power spectral density $S_q(f) \propto 1/f^{\alpha}$ with α between 1.0 and 1.25 [11–21] and noise magnitude $S_q(1 \text{ Hz}) \sim 10^{-5} - 10^{-7} \, e^2/\text{Hz}$. The standard microscopic picture of this noise is a distribution of two-level fluctuators (TLFs) [19,22,23] that can activate or tunnel between local minima in a potential energy landscape, leading to switching

behavior in the time domain and a Lorentzian power spectral density. A bath of TLFs with a broad distribution of characteristic rates gives rise to the ubiquitous 1/f noise.

Here, we describe measurements of charge noise in a charge-tunable qubit that departs slightly from the transmon regime. We find a charge noise power spectral density that is up to four orders of magnitude larger at 1 Hz than that seen in SETs, suggesting an unexpected dependence of the noise on device scale. Moreover, we observe a large number of discrete charge jumps in excess of 0.1e. The measured distribution of charge jumps is not compatible with charge motion over microscopic length scales, as described by the standard picture of dipolelike TLFs. Finally, the measured noise exponent $\alpha = 1.9$ is incompatible with the exponents reported for SETs, pointing to another noise mechanism. While our measured noise is strikingly different from that seen in SETs, it is consistent with reports of frequency noise in other superconducting qubits [24,25].

The device geometry is shown in Fig. 1. Each die consists of a charge-sensitive qubit and a charge-insensitive reference transmon coupled to a common $\lambda/2$ readout resonator. The devices were fabricated on high-resistivity silicon; the circuit ground plane, qubit islands, and all control and readout elements were made from sputtered niobium and defined using optical lithography and reactive ion etching. The Al-AlO_x-Al compound Josephson junctions of the qubits were fabricated using electron-beam lithography and double-angle evaporation [26,27].

The qubit parameters are $E_J/h = 10.8$ GHz at the flux-insensitive point and $E_C/h = 390$ MHz, corresponding to a qubit transition frequency $\omega_{10}/2\pi = 5.38$ GHz. The readout mode resonates at 6.744 GHz. The qubit is coupled to the resonator with a coupling strength of $g/2\pi = 100$ MHz and

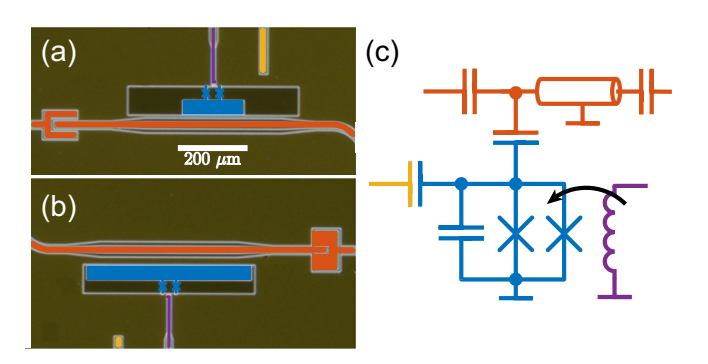


FIG. 1. Micrograph of the charge-sensitive qubit [(a) $E_C/h = 390$ MHz, $E_J/h = 10.8$ GHz] and the reference transmon [(b) $E_C/h = 230$ MHz, $E_J/h = 16$ GHz]. The qubit structures are shown in blue; the readout resonator and feedline are red; and the charge and flux bias lines are colored orange and purple, respectively. (c) Diagram of the qubit circuit.

the state is read out dispersively with a qubit state-dependent shift of $\chi/\pi=3.7$ MHz. The resonator is strongly coupled to the output port with a decay time $1/\kappa=75$ ns to allow for rapid repeated measurements. The offset charge is controlled through an on-chip capacitance to the qubit island of 100 aF, with a 20:1 voltage division at the millikelvin stage. The device is measured in a dilution refrigerator with a base temperature of 35 mK.

While typical transmon devices involve a ratio E_J/E_C in the range 50–100 [3,28], leading to a charge dispersion ranging from 10 kHz to 1 Hz, the ratio $E_J/E_C=28$ yields a charge dispersion $\Delta\omega_{10}/2\pi=600$ kHz. The qubit energy spectrum is given by $\overline{\omega_{10}}+\Delta\omega_{10}\cos(2\pi n_g)$, where $\overline{\omega_{10}}$ is the charge-averaged qubit frequency and n_g is the offset charge on the qubit island expressed in units of 2e [Fig. 2(a)]. The dependence of the qubit transition frequency on offset charge renders the device sensitive to quasiparticle (QP) poisoning [29]. Here, single QPs tunnel across the Josephson junctions on submillisecond timescales [24,25], changing n_g by 0.5 and giving rise to distinct parity bands in the qubit spectrum.

To measure fluctuations in the offset charge on the qubit island, we perform a series of Ramsey experiments at varying charge bias points using a pulse sequence that maps offset charge onto the population of the qubit excited state [Fig. 2(b)]. With QP tunneling rates far exceeding the repetition rate of the Ramsey experiments, we require the experiment to be independent of parity of the qubit island. The sequence begins with a broadband (40-ns-long) X/2 gate that addresses both parity bands. The qubit then undergoes free evolution for an interval t_i , accumulating the phase $\pm \Delta\omega_{10}t_i\cos 2\pi n_g$, where the two signs correspond to the two possible parity states. While the two parity states evolve in different directions around the equator of the Bloch sphere, they maintain the same projection onto the y axis. We set the idle time $t_i = \pi/\Delta\omega_{10}$ and use a final X/2 gate to map this projection onto the z axis of the Bloch sphere. Measurement

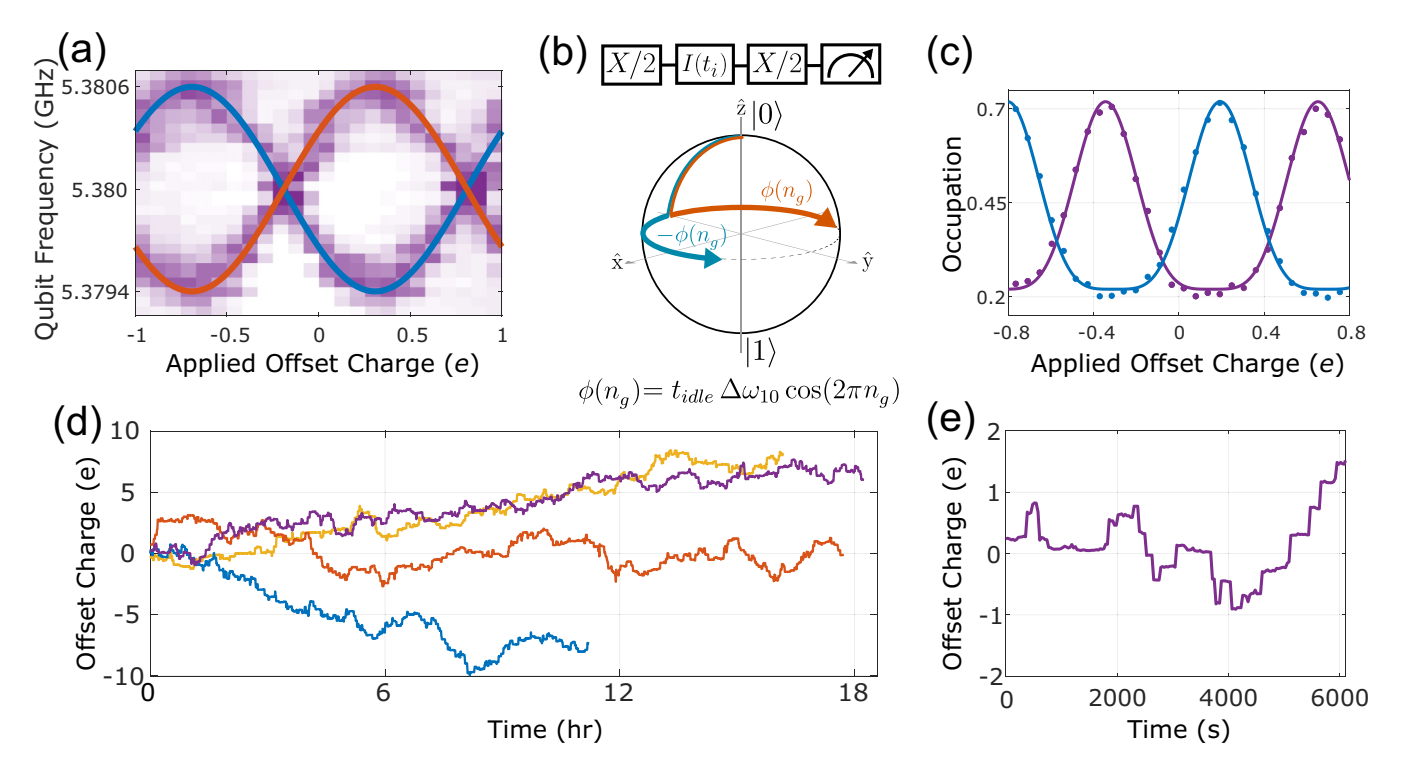


FIG. 2. Ramsey-based extraction of offset charge. (a) Qubit spectroscopy vs charge bias at the flux-insensitive point. As QP tunneling rates far exceed the experimental repetition rate, we observe both QP parity bands (red and blue traces). (b) Pulse sequence used to estimate the offset charge, along with a diagram of the trajectory of the qubit state vector on the Bloch sphere for the two values of QP parity. (c) Representative Ramsey-based charge tomography for two values of δn_g . The pulse sequence of (b) is repeated for a range of applied offset charge. From a fit to Eq. (1) we extract the change to the island offset charge δn_g due to intrinsic noise processes. (d) Time series of fluctuating offset charge. (e) Expanded view of measured δn_g . Frequent large-magnitude (>0.1e) jumps are clearly visible.

of the qubit finds an excited state probability

$$P_1 = \frac{1}{2}[d + \nu \cos(\pi \cos 2\pi n_g)],\tag{1}$$

where $n_g = n_g^{\rm ext} + \delta n_g$ is the sum of an applied gate charge $n_g^{\rm ext}$ and a fluctuating intrinsic offset charge δn_g and the parameters d and ν account for qubit decay during measurement and finite measurement visibility, respectively. Critically, P_1 is periodic in offset charge with period $n_g = 0.5$, and is thus insensitive to QP parity. We sweep the externally applied gate charge $n_g^{\rm ext}$ and determine δn_g by fitting the measured Ramsey data to Eq. (1). Using this technique, we can determine the offset charge to a precision of 0.02e over 20 s. Once δn_g is measured, we can then deterministically bias to any point in charge space.

Repeated Ramsey scans of this type generate a time series of fluctuating offset charge [Fig. 2(d)]. Interestingly, the charge trace shows occasional (once per \sim 250 s) extremely large discrete jumps >0.1e. The observed distribution of offset charge jumps is difficult to reconcile with a model of dipolelike microscopic TLFs. Note that, as Ramsey tomography is periodic in an offset charge of 1e, we can only determine changes in offset charge within the range [-0.5e, 0.5e); any larger jump is aliased to a reduced value of offset charge (e.g., a 0.6e change looks identical to a -0.4e change).

In order to characterize the fluctuating offset charge at higher frequency, we adopt a fast single-shot Ramsey protocol that simultaneously probes island parity and fluctuating offset charge [Fig. 3(a)]. An initial Ramsey sequence maps the two parity states to the north and south poles of the Bloch sphere. Single-shot measurement of the qubit state provides access to the QP parity of the qubit island. Following a short delay of $1 \mu s \sim 13/\kappa$ to allow the cavity to return to its ground state, we perform a second single-shot Ramsey experiment that maps offset charge to qubit population irrespective of island parity. We bias the qubit to the point of maximal charge sensitivity and perform an X/2 gate that rotates the qubit parity states to opposite sides of the equator of the Bloch sphere. Noise in the charge bias causes the two states to accumulate phase in opposite directions; however, a subsequent Y/2 gate maps the accumulated phase to the same polar angle on the Bloch sphere. Due to the presence of large jumps in offset charge on a few-minute timescale, we interleave with this sequence a separate Ramsey-based scan of offset charge every 15 s in order to compensate large jumps in offset charge. By repeating the two-step protocol with a duty cycle of 10 kHz, we generate two time series of single-shot measurement results, the first of which provides access to island parity and the second of which provides access to fluctuating offset charge. For each separate time series (QP parity or charge), we partition the time trace into two interleaved traces, compute the cross spectrum, and average over many measurement cycles to suppress quantum projection noise, after Refs. [30,31].

The power spectrum of QP parity [Fig. 3(b)] is Lorentzian with a characteristic frequency of 255 Hz set by the rate of QP tunneling onto or off of the qubit island; this QP poisoning rate is consistent with other reported values in the superconducting qubit literature [24,25]. For the charge noise results [Fig. 3(c)], we combine the fast single-shot Ramsey results with the low-frequency charge noise power spectral density

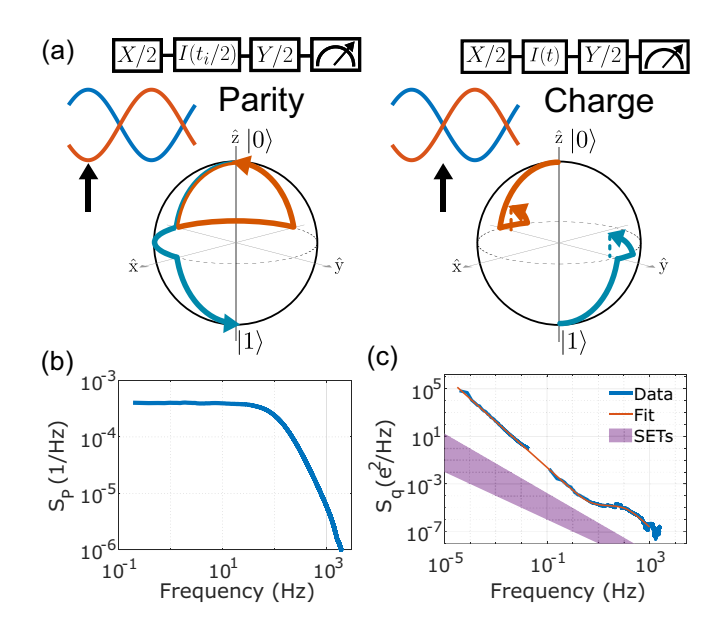


FIG. 3. (a) Pulse sequences for Ramsey-based single-shot measurement of QP parity and charge noise. In the first sequence, the qubit is biased to a parity-sensitive point; the X/2-idle-Y/2 sequence is designed to map QP parity to the north and south poles of the Bloch sphere. The sequence is immediately followed by a second experiment that maps fluctuating offset charge to qubit population. Here, the device is biased to the point of maximal charge sensitivity; following an initial X/2 pulse, states that reside on the two QP parity bands accumulate phase with opposite sign; a final Y/2 pulse maps the qubit state to the same polar angle on the Bloch sphere irrespective of QP parity. (b) Power spectral density of QP parity fluctuations. The spectrum is Lorentzian with a characteristic frequency at $\Gamma/2\pi = 255$ Hz. (c) Power spectral density of offset charge noise. The low-frequency portion of the spectrum is obtained from the time series presented in Fig. 2(d), while the high-frequency portion of the spectrum is derived from the single-shot protocol of (a). Residual QP tunneling dominates the spectrum above 10 Hz. The orange trace is a fit to the sum of a power-law spectrum $S_q(f) = A/f^{\alpha}$ and a single Lorentzian. We find $S_a(1 \text{ Hz}) = 2.9 \times 10^{-4} e^2/\text{Hz}$ and $\alpha = 1.93$.

obtained from the time series presented in Fig. 2(d). The power spectral density of offset charge fluctuations displays a $1/f^{\alpha}$ spectrum, with $S_q(1~{\rm Hz}) = 2.9 \times 10^{-4}~e^2/{\rm Hz}$ and $\alpha = 1.93$. The measured charge noise is inconsistent with a large body of literature on charge noise in SETs, both in the noise magnitude at 1 Hz and in the noise exponent.

While charge noise has not previously been reported on weakly charge-sensitive qubits of the transmon type, there are reports of frequency noise [24,25]. To compare our data to these prior experiments, we convert our measured offset charge to difference frequency using the relation $\delta f = |\Delta\omega_{10}\cos(2\pi n_g)|$. In this case, we find $S_{\delta f}(1 \text{ Hz}) = 5.9 \times 10^7 \text{ Hz}^2/\text{Hz}$ with noise exponent $\alpha = 1.76$, which closely matches the other measured values (after proper normalization to the same charge dispersion) of $S_{\delta f}(1 \text{ Hz}) = 8.1 \times 10^7 \text{ Hz}^2/\text{Hz}$ and $\alpha = 1.7$ [24], and $S_{\delta f}(1 \text{ Hz}) = 3.7 \times 10^7 \text{ Hz}^2/\text{Hz}$ and $\alpha = 1.70$ [25]. More details on this comparison can be found in the Supplemental Material [26]. While a conversion from frequency noise to charge noise is not possible due to nontrivial aliasing effects, the similar levels

of frequency noise seen in these three independent qubit measurements suggest a common noise mechanism, despite the fact that these measurements span a range of substrate materials (Si, this work; Al_2O_3 [24,25]), base metal (Nb, this work; Al [24,25]), and cavity architecture [two dimensional (2D), this work; 3D [24,25]].

As this noise is substantially larger than what is seen in SET devices, it is instructive to consider the differences between the two systems. First, SETs are operated in the voltage state, whereas transmons are operated in the superconducting state. Naively, one might expect to observe higher levels of noise in devices operated in the dissipative regime; SET measurements confirm this intuition, where higher-voltage bias results in larger noise [16,18]. The other notable distinction is the large qubit capacitor pad. For our charge-sensitive device, with qubit charging energy $E_C/h = 390$ MHz, the island dimensions are $40 \times 180 \ \mu \text{m}^2$. For typical SETs, the island dimensions are submicron and the charging energy is of order 40 GHz [32,33]. It is thus reasonable to consider whether the enhanced noise seen in our devices is related to the difference in device scale. In the most widely accepted pictures of low-frequency charge noise, the fluctuating offset charge is due to dipolelike TLFs involving the motion of a single electron charge over microscopic scales, with dipole moments of order 1 D [34]. Such dipolar fluctuators can only produce large changes in offset charge when they are located within a dipole length from the junction, which represents the boundary between the island and ground electrodes. For TLF with characteristic dipole moment of several debyes, this length is on the order of 1 Å. However, we observe a broad distribution of discrete jumps in offset charge, with many large jumps in excess of 0.1e. In Fig. 4 we plot the histogram of discrete charge jumps obtained from the time series in Fig. 2. In addition to a Gaussian central peak with width 0.02e set by the fit uncertainty in our Ramsey-based charge measurements, the histogram displays long tails corresponding to a large number of discrete charge jumps extending out to $\pm 0.5e$ (as described above, any larger charge jumps are aliased into this interval). The frequency of large-magnitude charge jumps suggests a model involving motion or drift of charge as opposed to fluctuations of individual localized TLF.

Indeed, the measured histogram is well modeled by random impingement of charge in the dielectric space between the qubit island and the ground electrode (see Fig. 4). Here, we perform a COMSOL simulation to calculate the induced charge on the qubit island associated with nucleation of a discrete 1e charge in the dielectric space between the qubit island and the circuit ground plane [Fig. 4(b)]. We then permit both charge polarities, which would correspond either to the nucleation of both positive and negative charged particles, or to the adsorption/desorption of a single charged species. We sample the entire ground-plane cavity with uniform density, appropriately alias the data to account for the finite dynamic range of our charge measurement (so that, e.g., 0.6e is mapped to -0.4e), and histogram the results. This naive simulation yields surprising agreement with the measured distribution of discrete charge jumps. Within a picture of impingement of discrete charges in the dielectric cavity of the qubit ground plane, the measured rate of charge jumps corresponds to a flux of charged particles of 17/cm² s, which could be due, e.g., to

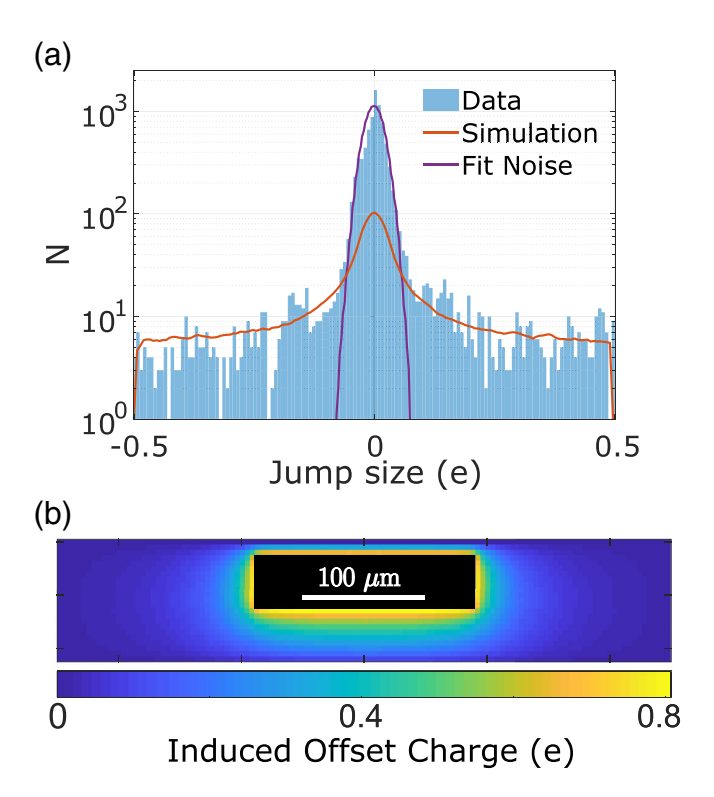


FIG. 4. (a) Histogram of discrete jumps in offset charge taken from 60 h of data. The histogram displays a large central peak and a long tail of large-magnitude jumps in offset charge. The purple trace is a Gaussian with width 0.02e, corresponding to the fit uncertainty in our Ramsey-based charge measurements, while the orange trace is obtained from the numerical simulation in (b), which shows the offset charge associated with impingement of discrete 1e charges in the dielectric space between the qubit island and ground. Here, the qubit island is shown in black and the field of view extends out to the circuit ground plane. The orange trace in (a) is generated by interpolating the simulation results and aliasing large offset charges to the interval [-0.5e, 0.5e), as occurs in the measured data.

a partial pressure of charged species of order 10^{-22} Torr. This pressure corresponds to roughly 0.4 ions in the Al box housing the sample, so the drift of charge might be better viewed as due to some element within the sample box that releases charge at a rate of ~ 500 particles per second. For example, the charge could be generated from the relaxation of strain in the printed circuit board (PCB) material used to couple signals into and out of the sample box or from the relaxation of strain in the dielectric substrate itself. Alternatively, it could be that free charge is generated by cosmic rays that are absorbed in the qubit substrate or in the material of the sample enclosure. However, the flux of cosmic rays is only $0.025/\text{cm}^2$ s at sea level [35–37], likely too low to account for the observed rate of discrete charge jumps.

Moreover, the large noise exponent is consistent with charge drift, as white current noise yields a charge spectrum that scales with frequency as $1/f^2$. For example, it could be that the apparent scale dependence of charge noise is due to a device-dependent sensing area to a fixed background drift of charge in the substrate or in the vacuum environment of the qubit, e.g., due to the motion of ions in the native oxide

of the silicon substrate [38,39] or to the trapping and release of charged particles in the substrate or surrounding dielectrics due to the relaxation of thermal strain. However, other models are possible, including fluctuating patch potentials on the island electrode [40,41], for which one would expect the charge noise to scale linearly with the area of the qubit island. We anticipate that a systematic study of the dependence of charge noise on device geometry will elucidate the underlying noise mechanism.

In conclusion, we have used a charge-sensitive variant of the transmon qubit to characterize anomalous low-frequency charge noise. The large noise magnitude, the noise exponent approaching 2, and the high density of large discrete charge jumps >0.1e are incompatible with the vast body of literature on charge noise in SETs yet consistent with prior reports of frequency noise in superconducting qubits, indicating a surprising dependence of charge noise on the device scale. A deeper understanding of charge noise could guide the development of noise mitigation strategies that will open the design space for superconducting qubits, leading to devices with stronger anharmonicity that are less prone to leakage errors and thus more amenable to scaling.

We acknowledge helpful discussions with Mark Eriksson and Nathan Holman. This research was supported by an appointment to the Intelligence Community Postdoctoral

Research Fellowship Program at University of Wisconsin-Madison, administered by Oak Ridge Institute for Science and Education through an interagency agreement between the US Department of Energy and the Office of the Director of National Intelligence. The research is based upon work supported by the Office of the Director of National Intelligence (ODNI), Intelligence Advanced Research Projects Activity (IARPA), via the US Army Research Office Grant No. W911NF-16-1-0114. The views and conclusions contained herein are those of the authors and should not be interpreted as necessarily representing the official policies or endorsements, either expressed or implied, of the ODNI, IARPA, or the US Government. Work by Y.R. and J.D. was performed under the auspices of the US Department of Energy by Lawrence Livermore National Laboratory under Contract No. DE-AC52-07NA27344. Y.R., J.D., B.C., and R. M. acknowledge partial support under LLNL-LDRD SI-16-004. The authors acknowledge use of facilities and instrumentation at the UW-Madison Wisconsin Centers for Nanoscale Technology partially supported by the NSF through the University of Wisconsin Materials Research Science and Engineering Center (DMR-1720415). This work was performed in part at the Cornell NanoScale Science & Technology Facility (CNF), a member of the National Nanotechnology Coordinated Infrastructure (NNCI), which is supported by the National Science Foundation (Grant No. NNCI-1542081), LLNL-JRNL-776205.

- [1] S. Boixo, S. V. Isakov, V. N. Smelyanskiy, R. Babbush, N. Ding, Z. Jiang, M. J. Bremner, J. M. Martinis, and H. Neven, Characterizing quantum supremacy in near-term devices, Nat. Phys. 14, 595 (2018).
- [2] C. Neill, P. Roushan, K. Kechedzhi, S. Boixo, S. V. Isakov, V. Smelyanskiy, A. Megrant, B. Chiaro, A. Dunsworth, K. Arya, R. Barends, B. Burkett, Y. Chen, Z. Chen, A. Fowler, B. Foxen, M. Giustina, R. Graff, E. Jeffrey, T. Huang *et al.*, A blueprint for demonstrating quantum supremacy with superconducting qubits, Science 360, 195 (2018).
- [3] J. Koch, T. M. Yu, J. Gambetta, A. A. Houck, D. I. Schuster, J. Majer, A. Blais, M. H. Devoret, S. M. Girvin, and R. J. Schoelkopf, Charge-insensitive qubit design derived from the Cooper pair box, Phys. Rev. A 76, 042319 (2007).
- [4] A. G. Fowler, Coping with qubit leakage in topological codes, Phys. Rev. A 88, 042308 (2013).
- [5] B. Douçot and L. B. Ioffe, Physical implementation of protected qubits, Rep. Prog. Phys. **75**, 072001 (2012).
- [6] M. T. Bell, J. Paramanandam, L. B. Ioffe, and M. E. Gershenson, Protected Josephson Rhombus Chains, Phys. Rev. Lett. 112, 167001 (2014).
- [7] M. T. Bell, W. Zhang, L. B. Ioffe, and M. E. Gershenson, Spectroscopic Evidence of the Aharonov-Casher Effect in a Cooper Pair Box, Phys. Rev. Lett. 116, 107002 (2016).
- [8] P. Groszkowski, A. D. Paolo, A. L. Grimsmo, A. Blais, D. I. Schuster, A. A. Houck, and J. Koch, Coherence properties of the 0-π qubit, New J. Phys. 20, 043053 (2018).
- [9] M. Kim, H. J. Mamin, M. H. Sherwood, K. Ohno, D. D. Awschalom, and D. Rugar, Decoherence of Near-Surface

- Nitrogen-Vacancy Centers Due to Electric Field Noise, Phys. Rev. Lett. **115**, 087602 (2015).
- [10] M. Brownnutt, M. Kumph, P. Rabl, and R. Blatt, Ion-trap measurements of electric-field noise near surfaces, Rev. Mod. Phys. 87, 1419 (2015).
- [11] B. M. Freeman, J. S. Schoenfield, and H. Jiang, Comparison of low frequency charge noise in identically patterned Si/SiO₂ and Si/SiGe quantum dots, Appl. Phys. Lett. **108**, 253108 (2016).
- [12] L. S. Kuzmin, P. Delsing, T. Claeson, and K. K. Likharev, Single-Electron Charging Effects in One-Dimensional Arrays of Ultrasmall Tunnel Junctions, Phys. Rev. Lett. 62, 2539 (1989).
- [13] G. Zimmerli, T. M. Eiles, R. L. Kautz, and J. M. Martinis, Noise in the Coulomb blockade electrometer, Appl. Phys. Lett. 61, 237 (1992).
- [14] G. Zimmerli, R. L. Kautz, and J. M. Martinis, Voltage gain in the single-electron transistor, Appl. Phys. Lett. 61, 2616 (1992).
- [15] E. H. Visscher, S. M. Verbrugh, J. Lindeman, P. Hadley, and J. E. Mooij, Fabrication of multilayer single-electron tunneling devices, Appl. Phys. Lett. 66, 305 (1995).
- [16] S. M. Verbrugh, M. L. Benhamadi, E. H. Visscher, and J. E. Mooij, Optimization of island size in single electron tunneling devices: Experiment and theory, J. Appl. Phys. 78, 2830 (1995).
- [17] D. Song, A. Amar, C. J. Lobb, and F. C. Wellstood, Advantages of superconducting Coulomb-blockade electrometers, IEEE Trans. Appl. Supercond. **5**, 3085 (1995).
- [18] H. Wolf, F. J. Ahlers, J. Niemeyer, H. Scherer, T. Weimann, A. B. Zorin, V. A. Krupenin, S. V. Lotkhov, and D. E. Presnov, Investigation of the offset charge noise in single electron tunneling devices, IEEE Trans. Instrum. Meas. 46, 303 (1997).

- [19] M. Kenyon, C. J. Lobb, and F. C. Wellstood, Temperature dependence of low-frequency noise in Al-Al₂O₃-Al single-electron transistors, J. Appl. Phys. **88**, 6536 (2000).
- [20] M. V. Gustafsson, A. Pourkabirian, G. Johansson, J. Clarke, and P. Delsing, Thermal properties of charge noise sources, Phys. Rev. B 88, 245410 (2013).
- [21] Y. Nakamura, Y. A. Pashkin, T. Yamamoto, and J. S. Tsai, Charge Echo in a Cooper-Pair Box, Phys. Rev. Lett. 88, 047901 (2002).
- [22] P. Dutta and P. M. Horn, Low-frequency fluctuations in solids: ¹/₄ noise, Rev. Mod. Phys. **53**, 497 (1981).
- [23] C. Müller, J. H. Cole, and J. Lisenfeld, Towards understanding two-level-systems in amorphous solids insights from quantum circuits, Rep. Prog. Phys. (2019), doi:10.1088/1361-6633/ab3a7e.
- [24] D. Ristè, C. C. Bultink, M. J. Tiggelman, R. N. Schouten, K. W. Lehnert, and L. DiCarlo, Millisecond charge-parity fluctuations and induced decoherence in a superconducting transmon qubit, Nat. Commun. 4, 1913 (2013).
- [25] K. Serniak, M. Hays, G. de Lange, S. Diamond, S. Shankar, L. D. Burkhart, L. Frunzio, M. Houzet, and M. H. Devoret, Hot Nonequilibrium Quasiparticles in Transmon Qubits, Phys. Rev. Lett. 121, 157701 (2018).
- [26] See Supplemental Material at http://link.aps.org/supplemental/ 10.1103/PhysRevB.100.140503 for further information.
- [27] The devices were originally designed to probe correlations of low-frequency flux and charge noise. These measurements set an upper limit on flux-charge correlations at 6%, and are described in the Supplemental Material.
- [28] J. A. Schreier, A. A. Houck, J. Koch, D. I. Schuster, B. R. Johnson, J. M. Chow, J. M. Gambetta, J. Majer, L. Frunzio, M. H. Devoret, S. M. Girvin, and R. J. Schoelkopf, Suppressing charge noise decoherence in superconducting charge qubits, Phys. Rev. B 77, 180502(R) (2008).
- [29] R. M. Lutchyn, L. I. Glazman, and A. I. Larkin, Kinetics of the superconducting charge qubit in the presence of a quasiparticle, Phys. Rev. B **74**, 064515 (2006).
- [30] F. Yan, J. Bylander, S. Gustavsson, F. Yoshihara, K. Harrabi, D. G. Cory, T. P. Orlando, Y. Nakamura, J. S. Tsai, and W. D. Oliver, Spectroscopy of low-frequency noise and its temperature dependence in a superconducting qubit, Phys. Rev. B 85, 174521 (2012).
- [31] C. M. Quintana, Y. Chen, D. Sank, A. G. Petukhov, T. C. White, D. Kafri, B. Chiaro, A. Megrant, R. Barends, B. Campbell, Z. Chen, A. Dunsworth, A. G. Fowler, R. Graff, E. Jeffrey,

- J. Kelly, E. Lucero, J. Y. Mutus, M. Neeley, C. Neill, P. J. J. OMalley, P. Roushan, A. Shabani, V. N. Smelyanskiy, A. Vainsencher, J. Wenner, H. Neven, and J. M. Martinis, Observation of Classical-Quantum Crossover of 1/*f* Flux Noise and its Paramagnetic Temperature Dependence, Phys. Rev. Lett. 118, 057702 (2017).
- [32] R. J. Schoelkopf, P. Wahlgren, A. A. Kozhevnikov, P. Delsing, and D. E. Prober, The radio-frequency single-electron transistor (rf-SET): A fast and ultrasensitive electrometer, Science 280, 1238 (1998).
- [33] A. Aassime, G. Johansson, G. Wendin, R. J. Schoelkopf, and P. Delsing, Radio-Frequency Single-Electron Transistor as Read-out Device for Qubits: Charge Sensitivity and Backaction, Phys. Rev. Lett. 86, 3376 (2001).
- [34] J. M. Martinis, K. B. Cooper, R. McDermott, M. Steffen, M. Ansmann, K. D. Osborn, K. Cicak, S. Oh, D. P. Pappas, R. W. Simmonds, and C. C. Yu, Decoherence in Josephson Qubits from Dielectric Loss, Phys. Rev. Lett. 95, 210503 (2005).
- [35] I. G. Nolt, J. V. Radostitz, M. Carlotti, B. Carli, F. Mencaraglia, and A. Bonetti, Cosmic-ray backgrounds in infrared bolometers, Int. J. Infrared Millimeter Waves 6, 707 (1985).
- [36] M. Lanfranchi, B. Carli, A. Gignoli, C. Lee, and M. Ridolfi, Cosmic-ray flux detected by an IR bolometer operated on board of a stratospheric aircraft, Infrared Phys. Technol. 40, 379 (1999).
- [37] K. Karatsu, A. Endo, J. Bueno, P. J. de Visser, R. Barends, D. J. Thoen, V. Murugesan, N. Tomita, and J. J. A. Baselmans, Mitigation of cosmic ray effect on microwave kinetic inductance detector arrays, Appl. Phys. Lett. 114, 032601 (2019).
- [38] V. Gorodokin and D. Zemlyanov, Metallic contamination in silicon processing, in 2004 23rd IEEE Convention of Electrical and Electronics Engineers in Israel (IEEE, Piscataway, NJ, 2004), pp. 157–160.
- [39] I. Constant, F. Tardif, and J. Derrien, Deposition and removal of sodium contamination on silicon wafers, Semicond. Sci. Technol. **15**, 61 (2000).
- [40] Q. A. Turchette, D. Kielpinski, B. E. King, D. Leibfried, D. M. Meekhof, C. J. Myatt, M. A. Rowe, C. A. Sackett, C. S. Wood, W. M. Itano, C. Monroe, and D. J. Wineland, Heating of trapped ions from the quantum ground state, Phys. Rev. A 61, 063418 (2000).
- [41] L. Deslauriers, P. C. Haljan, P. J. Lee, K. A. Brickman, B. B. Blinov, M. J. Madsen, and C. Monroe, Zero-point cooling and low heating of trapped ¹¹¹Cd⁺ ions, Phys. Rev. A 70, 043408 (2004).